Current Biology 20, 1099–1103, June 22, 2010 ©2010 Elsevier Ltd All rights reserved DOI 10.1016/j.cub.2010.04.045

Report

Robust Growth of *Escherichia coli*

Ping Wang,[1,5] Lydia Robert,[2,3,5] James Pelletier,[1] Wei Lien Dang,[1] Francois Taddei,[2] Andrew Wright,[4] and Suckjoon Jun[1,*]

[1]FAS Center for Systems Biology, Harvard University, 52 Oxford St, Cambridge, MA 02138, USA

[2]Université Paris Descartes, Faculté de Médecine, Inserm U571, 156 rue de Vaugirard, 75015 Paris, France

[3]AgroParisTech ENGREF, 19 avenue du Maine, F 75732 Paris, France

[4]Department of Molecular Biology and Microbiology, Tufts University School of Medicine, 136 Harrison Avenue, Boston, MA 02111, USA

Summary

The quantitative study of the cell growth [1–5] has led to many fundamental insights in our understanding of a wide range of subjects, from the cell cycle [6–9] to senescence [10]. Of particular importance is the growth rate, whose constancy represents a physiological steady state of an organism. Recent studies, however, suggest that the rate of elongation during exponential growth of bacterial cells decreases cumulatively with replicative age for both asymmetrically [11] and symmetrically [12, 13] dividing organisms, implying that a "steady-state" population consists of individual cells that are never in a steady state of growth. To resolve this seeming paradoxical observation, we studied the long-term growth and division patterns of *Escherichia coli* cells by employing a microfluidic device designed to follow steady-state growth and division of a large number of cells at a defined reproductive age. Our analysis of approximately 10^5 individual cells reveals a remarkable stability of growth whereby the mother cell inherits the same pole for hundreds of generations. We further show that death of *E. coli* is not purely stochastic but is the result of accumulating damages. We conclude that *E. coli*, unlike all other aging model systems studied to date, has a robust mechanism of growth that is decoupled from cell death.

Results and Discussion

To follow a large number of cells inheriting the same pole and their progeny for many generations, we employed a high-throughput, continuous, microfluidic liquid-culture device that we built by using a standard soft-lithographic technique that others had developed for cell biology studies [14–17]. Our device consists of a series of growth channels, oriented at right angles to a trench through which growth medium is passed at a constant rate (Figure 1A). This constant flow results in diffusion of fresh medium into the growth channels as well as removal of cells as they emerge from the channels into the main trench (Figure 1A). We measured the timescale of nutrient uptake by *E. coli* by using the fluorescent glucose analog (2-NBDG) and found that diffusion into the channels is much faster (~1 s) than the timescale of nutrient uptake (~2–3 min; Supplemental Experimental Procedures, available online), ensuring steady-state conditions for all cells. The cell at the end of the growth channel, distal to the trench, is referred to as the "old-pole mother cell" (or mother cell) because one of its poles, abutting the end of the channel, is inherited from one generation to the next (Figure 1A). The diameter of the growth channels prevents the mother cell from moving around. The replicative age of the mother cell, defined as the number of consecutive divisions from the young-pole daughter cell [12], increases by one generation at each cell division (Figure 1B). It is noteworthy that this device, which we call the "mother machine," allows us to follow cells for numbers of generations that are orders of magnitude greater than has been possible with other single-celled organisms, including *Saccharomyces cerevisiae* [18] and *E. coli* [12, 13] (see Experimental Procedures; Movie S1 and Movie S2).

We studied two distantly related strains of *E. coli*, B/r and MG1655, which constitutively express yellow fluorescent protein (YFP) from a chromosomal copy of the *yfp* gene, allowing visualization of the cells via live microscopy (Figure 1C). A typical time series of a single growth channel from the beginning of the experiment until death of the mother cell is shown in the top panel of Figure 1D (which we constructed from the time series images by following the growth channel indicated by the dotted yellow box in Figure 1C; see Movie S2). This temporal montage shows the fluorescence level (YFP) of the mother cell and her progeny over time during the reproductive lifetime of the mother cell (Figure 1D [middle panel]). A cell length-versus-time curve was constructed for every cell in all of our experiments (e.g., Figure 1D, bottom panel). This curve is well approximated by a straight line in a semi-log plot (see the inset of Figure 1D). That is, each interval between birth and division can be fitted via a single exponential function to give the growth rate of the cell at that replicative age. The spikes that appear at random intervals in the size distribution are the result of limited filamentation, as discussed in detail below.

The growth rate of individual cells showed a striking long-term stability over hundreds of generations, as indicated by the average-growth-rate-versus-replicative-age curves of the old-pole mother cells (Figure 2). The growth rate remained constant under our experimental conditions, for both MG1655 and B/r. In contrast to this long-term stability, the growth rate of the old-pole mother cell showed only weak correlation between two consecutive cell cycles. Mother cells exhibited fast fluctuations with a timescale of less than one generation and a Gaussian distribution (Figure 2 inset; Figure 3A). The daughter cells also showed the same growth-rate statistics as the mother cells, as we summarize in Figures S1 and S2. In other words, the cell "forgets" immediately upon division how fast it was growing in the previous cell cycle.

The observed stable growth is mirrored by the stable protein synthesis reflected in the long-term constant fluorescence level of the mother cell and its progeny (Figure 1D, top two panels). Like the growth rate, the YFP fluorescence level also shows a short-time correlation of one to two generations, consistent with previous findings in *E. coli* and human cells

*Correspondence: sjun@cgr.harvard.edu

[5]These authors contributed equally to this work

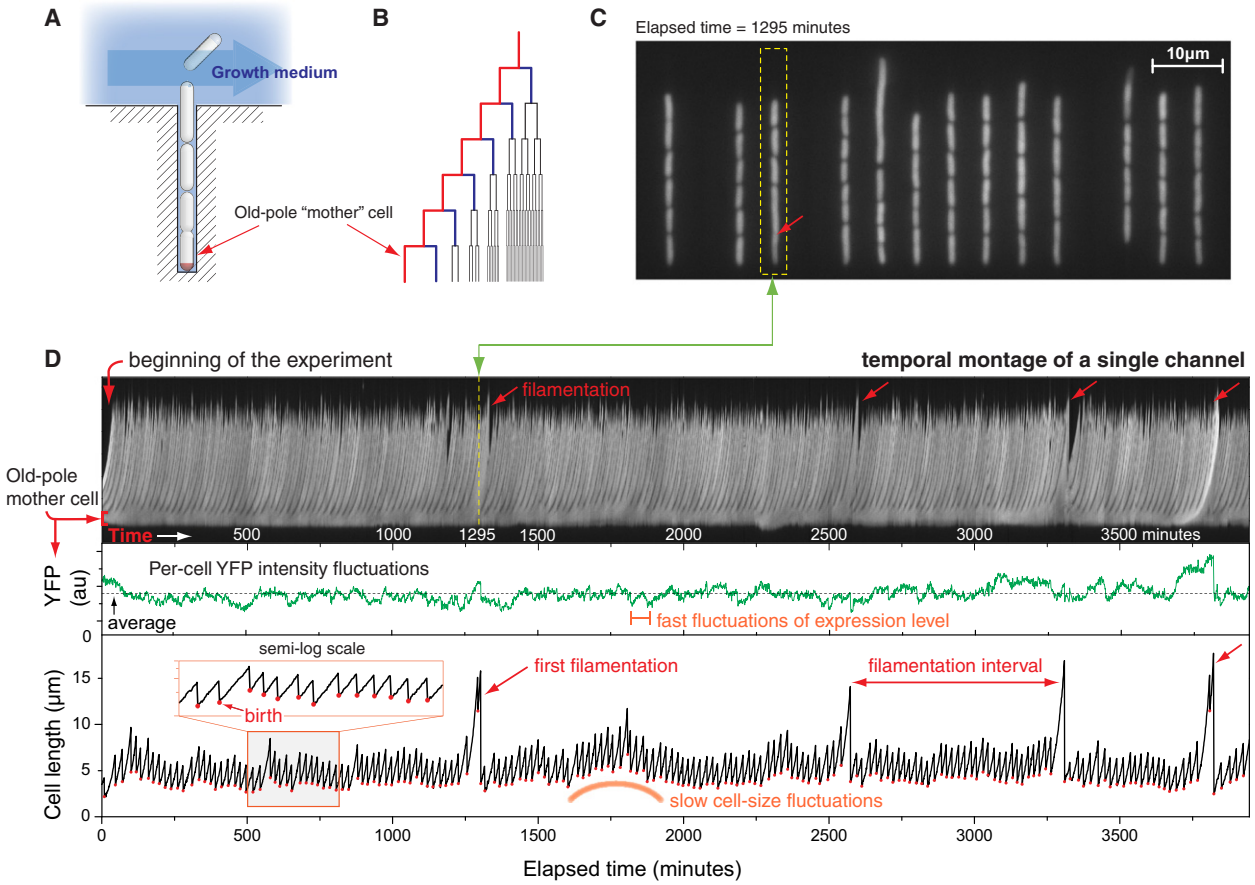

Figure 1. The "Mother Machine" and High-Throughput Observation of the Mother Cells

(A) Schematic illustration of the microfluidic mother machine. The old-pole mother cell is trapped at the end of the growth channel.

(B) The outermost branch of the lineage tree represents the old-pole mother cell and her progeny.

(C) Snapshot of a typical field of view.

(D) Top panel: temporal montage of a single growth channel (within the dotted yellow box in [C]) from the beginning to the end of the experiment. The stable band on the bottom of the montage is the old-pole mother cell, whereas the "feather" of the montage shows the growth and escape of her progeny. Middle panel: the average YFP intensity of the mother cell fast fluctuating around the mean without decay over time. Bottom panel: cell length versus time of the old-pole mother cell, which shows occasional spikes (filamentations). In all three panels, the *x* axis represents time in minutes.

[19, 20] (Figure 3B). Our results showing the long-term stability of growth and protein synthesis, accompanied by their short-term memory, argue strongly against a built-in growth-based aging mechanism in *E. coli*. In other words, in *E. coli* cultures, all cells will be in the same steady state of growth and will be indistinguishable from one another regardless of their replicative age.

Although our experiments unambiguously show that growth and protein synthesis are characterized by short-term correlations, surprisingly, further analysis revealed an unexpected long-term correlation that spans dozens of generations. Specifically, at a critical replicative age of the first 50 generations, we noted a striking increase in filamentation of the mother cells of MG1655 (the "spikes" seen in Figure 1D bottom panel; Figure 3C; Figure S3). Importantly, the filamentation rate of the daughter cells remained practically constant, and thus the increased filamenation of the mother cell cannot be due to illumination. This means that the mother cell must inherit an unknown "factor" that serves as a long-term memory from one generation to the next and causes filamentation independently of growth and protein synthesis. Indeed, filamentation in Figure 1D occurs at intervals such that its distribution follows a power law characterized by a long tail (Figure 3D). (Note that random events will produce an exponential ["memory-less"] distribution.) Such a long-term effect could not have been detected by more conventional timelapse experiments of an exponentially growing population because it requires observation of the mother cell's inheriting the same old pole for hundreds of generations.

Because filamentation is a hallmark of the SOS response in bacteria, we asked how its suppression would affect our observation of filamentation. For this purpose we constructed an MG1655 derivative carrying a *lex*A allele, *lex*A3, whose protein product constitutively represses SOS gene expression even under conditions of DNA damage. Although the *lexA3* mutant behaved virtually the same as MG1655 in terms of a constant growth rate, its filamentation rate, which was constant at approximately 1%, was significantly reduced, as expected. Note that B/r lacks *sulA*, a key SOS gene that inhibits cell division during the SOS response, and also shows a similar low filamentatin rate (Figure S3). A more important difference between *lex*A3 and MG1655 is that, with a constant death rate of 2.7% per cell per generation, the population of the *lex*A3 mutant cells decayed exponentially (Figure 4).

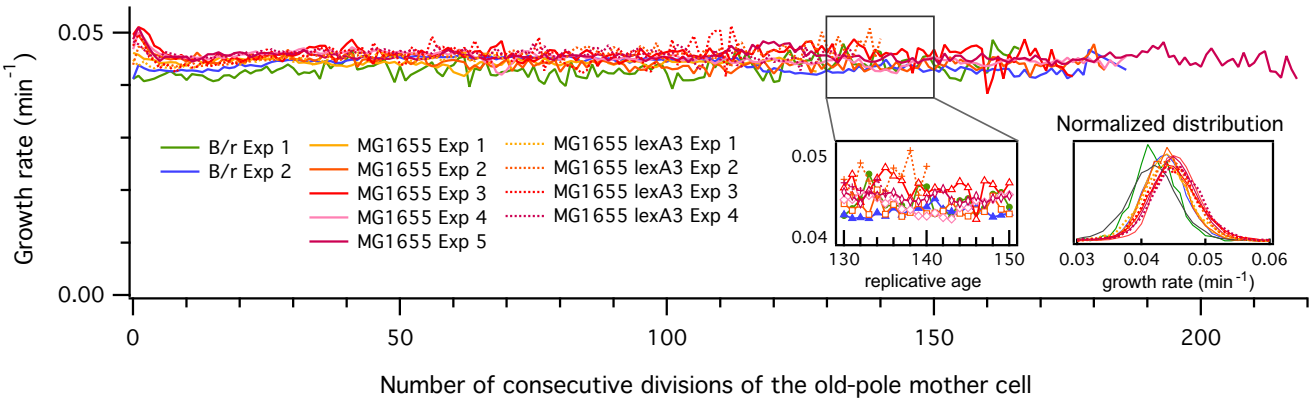

Figure 2. Long-Term Stability of Growth Rate in *E. coli*

The elongation rate does not show any cumulative decrease over 200 generations in any of the three strains (B/r, MG1655, or MG1655 lexA3). The growth rates show fast fluctuations with short-term correlation and follow a Gaussian distribution. These eleven curves represent more than $\sim 10^5$ individual mother cells, namely, $\sim 10^7$ measured cell lengths.

These findings have important implications for the cause of cell death. That is, the death of the *lexA3* mutant is random and requires the SOS response for survival. The much slower death rate of wild-type MG1655 cannot simply be due to a purely stochastic, age-independent fluctuation in DNA damage or metabolism; otherwise, we would have observed an exponential decay like that of the *lex*A3 mutant (Figure 4). Instead, death of MG1655 is probably caused by a growth-independent inheritance and accumulation of a lethal "factor" as indicated by the long-term correlation observed in the mother cell described above. It is possible that this "factor" corresponds to protein aggregates that are asymmetrically distributed in *E. coli* and which are described in recent work [13, 21]. An alternative but not mutually exclusive idea is that the physically aging cell wall at the pole accumulates defects as a result of its metabolic inertness [22], which also could be linked to the lethal element.

In previous work by Stewart et al. [12], it was found that the growth rate of the mother cell decreased cumulatively with replicative age, about 2% per generation. Although our results show otherwise, this could be due to the differences in the experimental conditions, e.g., two-dimensional surface on an agar pad (Stewart et al.) versus one-dimensional growth channel where fresh liquid medium is constantly supplied (current study). In addition, we excluded the data from the first ten generations of replicative age to ensure that our results reflect steady-state growth conditions. Nevertheless, we note that the average generation times of the mother cells of B/r, MG1655, and *lex*A3 mutant are in precise agreement with the generation time measured from the growth curves of the liquid culture (see Experimental Procedures). This strongly argues that, in our study, it is unlikely that there is a decrease of the growth rate of the mother cell regardless of its replicative age, i.e., all cells are in the same steady state of growth.

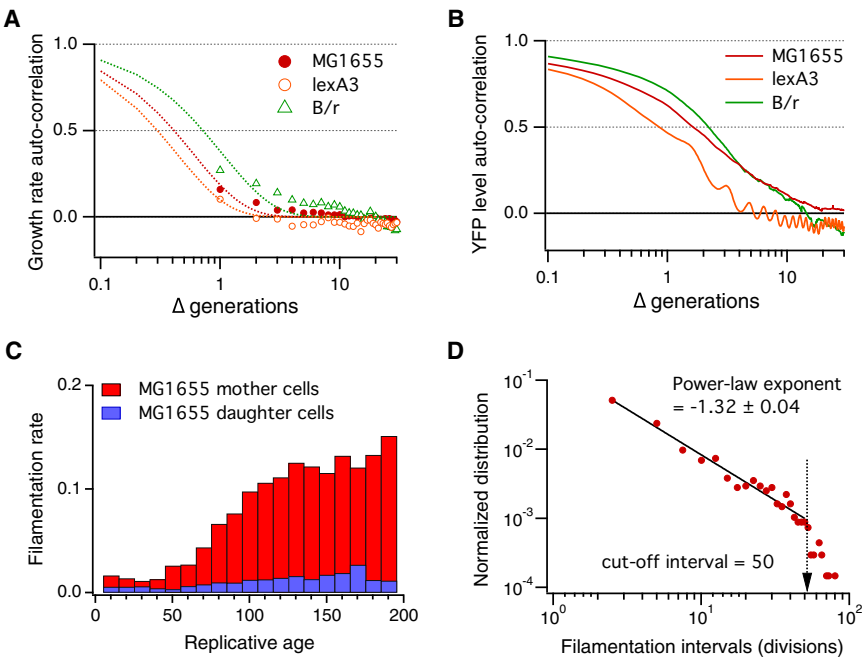

Figure 3. Short-Term Correlation of Growth Rates versus Long-Term Inheritance of a "Factor" in the Mother Cell

(A) Autocorrelation function of growth rates showing less than one generation of correlation time. The dashed lines are fit to the data via a single exponential function (to guide the eye): exp(−0.7x), exp(−0.43x), and exp(−x) for MG1655, MG1655 *lexA*3, and B/r, respectively.

(B) Autocorrelation function of YFP level also showing 1–2 generations of correlation time.

(C) Filamentation rate of MG1655. At a critical replicative age of the first 50 generations, the filamentation rate of the mother cell starts to increase, in contrast to the daughter cells, which continue to divide normally.

(D) A power-law distribution of filamentation intervals characterized by a long tail. Together with the increasing filamentation rate in (C), this implies a long-term memory that is independent of the observed stable growth and protein synthesis shown in Figures 1 and 2.

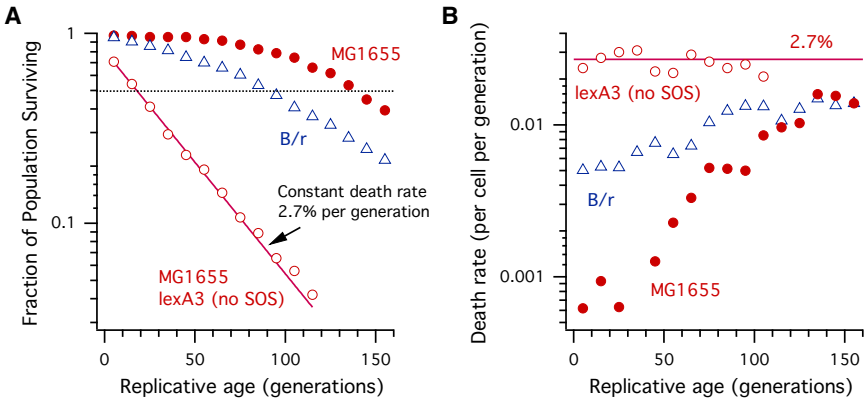

Figure 4. Survival and Mortality-Rate Analysis Showing Aging of *E. coli*

(A) Survival curves of B/r, MG1655, and MG1655 *lex*A3 mutant (no SOS response). The pure exponential decay of the MG1655 *lex*A3 population with time allows us to directly extract 2.7% of the constant death rate per generation in the absence of the SOS response. The higher survival rate of MG1655 is due to the SOS response. The dotted horizontal line represents 50% decay of the initial populations.

(B) Death rate computed by numerical differentiation of the survival curves in (A). Both B/r and MG1655 show increasing mortality rates, whereas MG1655 *lex*A3 shows a constant 2.7% rate of cell death.

In summary, using the microfluidic mother machine, we have shown a striking constant growth rate of the mother cells of *E. coli* and their immediate sister cells for hundreds of generations. Also, from the qualitative difference in the death rate between MG1655 and its *lexA3* mutant derivative, we concluded that the death of *E. coli* cells cannot be due to random events such as DNA damage but must be a consequence of growth-independent accumulation of a lethal element. These observations have been made possible because the mother machine allows us to follow a large number of cells for a long time at the single-cell level in a precisely controlled environment and produces amounts of data comparable to data from studies at a population level (e.g., FACS). Our experimental approach can be directly and immediately applied to a wide range of problems.

In our view, the most important lesson from our study is that *E. coli* must have a very robust mechanism of growth. The next major challenge, then, is to understand the origin of the stability of bacterial growth. Understanding it at the systems level may shed a new light on an important related question, i.e., how replication and division are coupled via growth and coordinated robustly in bacteria in the absence of eukaryotic-like checkpoints [23].

Experimental Procedures

Growth Condition, Microscopy, and Microfluidics

Cultures were grown overnight in Luria-Bertani (LB) at 37°C. The next day, 30 μl of the overnight culture was back diluted in 3 ml of fresh LB at 37°C. At OD_{450} = 0.2 to 0.3 (or OD_{600} = 0.1 to 0.15), the cell culture was 10× concentrated by centrifugation for injection into the mother machine. The cells were loaded by diffusion until more than 80% of the channels were filled with the cells. Fresh LB medium was infused by a syringe pump. For each experiment, images were acquired from 10–12 fields at 1 min intervals via NIS-Elements software and a Nikon Eclipse Ti fluorescence microscope equipped with a motorized stage and a CCD camera (Photometrics CoolSnap HQ2). We tested a wide range of dosages by varying the exposure time (1.5–4.0 s) and the intensity of the illumination light by using neutral density filters (ND32 to ND128; ND128 means that only 1/128 of the illumination light is used for imaging). Above ND32 and up to 2 s of exposure time, the growth rate and generation time measured in the mother machine precisely agreed with that measured from the growth curve for both *E. coli* strains B/r and MG1655 used in our studies: MG1655 = 20.9 ± 0.3 min, MG1655 *lex*A3 = 20.7 ± 0.8 min, B/r D = 22.6 ± 0.4 min.

Our device consists of 4000 growth channels and an automated microscope stage, which we use to continuously scan 10–12 fields of view for 72 hr at 1 min intervals (Movie S1). Because each field of view contains ~10^2 cells at 100× magnification (Figure 1C), we acquired and processed images of ~10^6–10^7 individual cells per experiment. See Supplemental Experimental Procedures for more details.

Image Analysis and Data Acquisition

Using C++, we designed custom software was to analyze time-lapse images. Our software has a user-friendly interface similar to that of ImageJ, as shown below. Because each experiment generated about 50,000–100,000 images, each containing ~10^2 cells, we analyzed typically ~10^7 cells per each time-lapse experiment. The current version of our software can complete analysis in about 3–5 hr on a standard desktop PC, which is significantly faster than other software developed with more high-level programming languages such as Matlab. We performed segmentation of cells directly on fluorescence images by finding basins of intensity along the channel direction.

Bacterial Strains

The wild-type strains of *Escherichia coli* MG1655 and B/r D were modified so that they expressed the gene encoding the yellow fluorescent protein (YFP) under the control of the constitutive promoter λP_R (gene construct from M. Elowitz [24]). The YFP gene, along with a chloramphenicol resistance gene, was inserted in the *int*C locus by P1 transduction from M. Elowitz's MRR strain (Elowitz 2002) and selection for chloramphenicol resistance. The lexA3 allele, present in strain RB258 [25], was introduced into MG1655, along with the closely linked marker malE::Tn5, by P1 transduction, with selection for kanamycin resistance. The MG1655 strain used is the poorly motile strain that does not contain an IS*1* insertion sequence element in the regulatory region of the *flhD* promoter [26] (CGSC 6300 of the *E. coli* Genetic Stock Center).

Autocorrelation Function

The normalized autocorrelation function A(Δt) has been calculated as follows:

$$A(\Delta t) = \left\langle \left(I(t+\Delta t) - \langle I(t+\Delta t)\rangle_t\right)\cdot\left(I(t) - \langle I(t)\rangle_t\right)\right\rangle_i \Big/ \left\langle \left\langle \left(I(t) - \langle I(t)\rangle_t\right)^2\right\rangle_t\right\rangle_i, \quad (1)$$

where $I(t)$ denotes the quantity of interest at time t (e.g., YFP intensity, cell length). $\langle\rangle_t$ and $\langle\rangle_i$ denote average over time and cells, respectively. From the typical timescale of decay of the (normalized) autocorrelation function, we can estimate how long the memory of the process lasts, for example, by measuring how fast it drops from 1 to 0.5. If A(Δt) decays exponentially as $\exp(-t/\tau)$, the inverse decay constant τ is defined as the correlation time of the process. However, if A(Δt) decays slowly, e.g, as a power-law $t^{-\alpha}$, where α is the exponent, there is no intrinsic timescale associated with the process. In this case, the process is said to have a long-term memory.

Filamentation

We considered a cell to be filamentous if its new-born cell size was larger than the population average by more than 2σ, where σ is the standard deviation of the cell-size distribution. In our experiments, filaments were visually obvious (Figures 1C and 1D) and well-separated from the normal cells in the size distributions (Figure S2B), and our results are insensitive to the choice of the threshold. To compute the filamentation intervals, we only counted intervals between new filamentations developed from a normal sized cell. For example, the double spikes around 1250 min in Figure 1D are counted as a single filamentation event.

Supplemental Information

Supplemental Information include Supplemental Experimental Procedures, four figures, and two movies and can be found with this article online at doi:10.1016/j.cub.2010.04.045.

Acknowledgments

We thank Irene Chen, Philippe Cluzel, Petra Levin, Steve Sandler, Bodo Stern for critical reading. We are particularly grateful to Andrew Murray for numerous stimulating and invaluable discussions on our manuscript. We also thank J.D. Deng (Harvard cleanroom), Peter Galajda, Daan Kiviet, Ariel Linder, Sander Tans, and Doug Weibel for helpful discussions on the development of microfluidic device in the early stage of this work, and we thank Robert Rioux (Whitesides lab) for help with chemical treatment of the PDMS device. This work was supported by Bauer Fellowship from Harvard University and the National Institutes of Health grant P50GM068763 (S.J.).

Received: March 24, 2010
Revised: April 18, 2010
Accepted: April 19, 2010
Published online: May 27, 2010

References

1. Monod, J. (1949). The growth of bacterial cultures. Annu. Rev. Microbiol. *3*, 371–394.
2. Schaechter, M., Maaloe, O., and Kjeldgaard, N.O. (1958). Dependency on medium and temperature of cell size and chemical composition during balanced growth of *Salmonella typhimurium*. J. Gen. Microbiol. *19*, 592–606.
3. Kjeldgaard, N.O., Maaloe, O., and Schaechter, M. (1958). The transition between different physiological states during balanced growth of *Salmonella typhimurium*. J. Gen. Microbiol. *19*, 607–616.
4. Helmstetter, C.E., and Cooper, S. (1968). DNA Synthesis during the division cycle of rapidly growing *Escherichia coli* B/r. J. Mol. Biol. *31*, 507–518.
5. Donachie, W.D. (1968). Relationship between cell size and time of initiation of DNA replication. Nature *219*, 1077–1079.
6. Nurse, P. (1975). Genetic control of cell size at cell division in yeast. Nature *256*, 547–551.
7. Neidhardt, F.C. (1999). Bacterial growth: Constant obsession with dN/dt. J. Bacteriol. *181*, 7405–7408.
8. Weart, R.B., Lee, A.H., Chien, A., Haeusser, D.P., Hill, N.S., and Levin, P.A. (2007). A metabolic sensor governing cell size in bacteria. Cell *130*, 335–347.
9. Tzur, A., Kafri, R., LeBleu, V.S., Lahav, G., and Kirschner, M.W. (2009). Cell growth and size homeostasis in proliferating animal cells. Science *325*, 167–171.
10. Henderson, K.A., and Gottschling, D.E. (2008). A mother's sacrifice: What is she keeping for herself? Curr. Opin. Cell Biol. *20*, 723–728.
11. Ackermann, M., Stearns, S.C., and Jenal, U. (2003). Senescence in a bacterium with asymmetric division. Science *300*, 1920.
12. Stewart, E.J., Madden, R., Paul, G., and Taddei, F. (2005). Aging and death in an organism that reproduces by morphologically symmetric division. PLoS Biol. *3*, e45.
13. Winkler, J., Seybert, A., Konig, L., Pruggnaller, S., Haselmann, U., Sourjik, V., Frangakis, A.S., Mogk, A., and Bukaru, B. (2010). Quantitative and spatio-temporal features of protein aggregation in Escherichia coli and consequences on protein quality control and cellular ageing. EMBO J. *29*, 910–923.
14. Balaban, N.Q., Merrin, J., Chait, R., Kowalik, L., and Leibler, S. (2004). Bacterial persistence as a phenotypic switch. Science *305*, 1622–1625.
15. Balagadde, F.K., You, L., Hansen, C.L., Arnold, F.H., and Quake, S.R. (2005). Long-term monitoring of bacteria undergoing programmed population control in a microchemostat. Science *309*, 137–140.
16. Lu, T., Shen, T., Bennett, M.R., Wolynes, P.G., and Hasty, J. (2007). Phenotypic variability of growing cellular populations. Proc. Natl. Acad. Sci. USA *104*, 18982–18987.
17. Weibel, D.B., DiLuzio, W.R., and Whitesides, G.M. (2007). Microfabrication meets microbiology. Nat. Rev. Microbiol. *5*, 209–218.
18. Mortimer, R.K., and Johnston, J.R. (1959). Life span of individual yeast cells. Nature *183*, 1751–1752.
19. Rosenfeld, N., Young, J.W., Alon, U., Swain, P.S., and Elowitz, M.B. (2005). Gene regulation at the single-cell level. Science *307*, 1962–1965.
20. Sigal, A., Milo, R., Cohen, A., Geva-Zatorsky, N., Klein, Y., Liron, Y., Rosenfeld, N., Danon, T., Perzov, N., and Alon, U. (2006). Variability and memory of protein levels in human cells. Nature *444*, 643–646.
21. Lindner, A.B., Madden, R., Demarez, A., Stewart, E.J., and Taddei, F. (2008). Asymmetric segregation of protein aggregates is associated with cellular aging and rejuvenation. Proc. Natl. Acad. Sci. USA *105*, 3076–3081.
22. den Blaauwen, T., de Pedro, M.A., Nguyen-Disteche, M., and Ayala, J.A. (2008). Morphogenesis of rod-shaped sacculi. FEMS Microbiol. Rev. *32*, 321–344.
23. Wang, J.D., and Levin, P.A. (2009). Metabolism, cell growth and the bacterial cell cycle. Nat. Rev. Microbiol. *7*, 822–827.
24. Elowitz, M.B., Levine, A.J., Siggia, E.D., and Swain, P.S. (2002). Stochastic gene expression in a single cell. Science *297*, 1183–1186.
25. Braun, R.E., and Wright, A. (1986). DNA methylation differentially enhances the expression of one of the two E. coli dnaA promoters in vivo and in vitro. Mol. Gen. Genet. *202*, 246–250.
26. Barker, C.S., Prüss, B.M., and Matsumura, P. (2004). Increased motility of *Escherichia coli* by insertion sequence element integration into the regulatory region of the flhD operon (MG1655). J. Bacteriol. *186*, 7529–7537.

Current Biology Volume *20*

Supplemental Information

Robust Growth of *Escherichia coli*

Ping Wang, Lydia Robert, James Pelletier, Wei Lien Dang, Francois Taddei, Andrew Wright, and Suckjoon Jun

Figure S1, related to Figure 2. Statistics of the elongation (growth) rate, generation time, newborn cell size for B/r and MG1655. (**A, B**) elongation rate, (**C, D**) generation time, (**E, F**) newborn cell size. The histograms are normalized for direct comparison such that the integrated area under the distribution becomes 1.

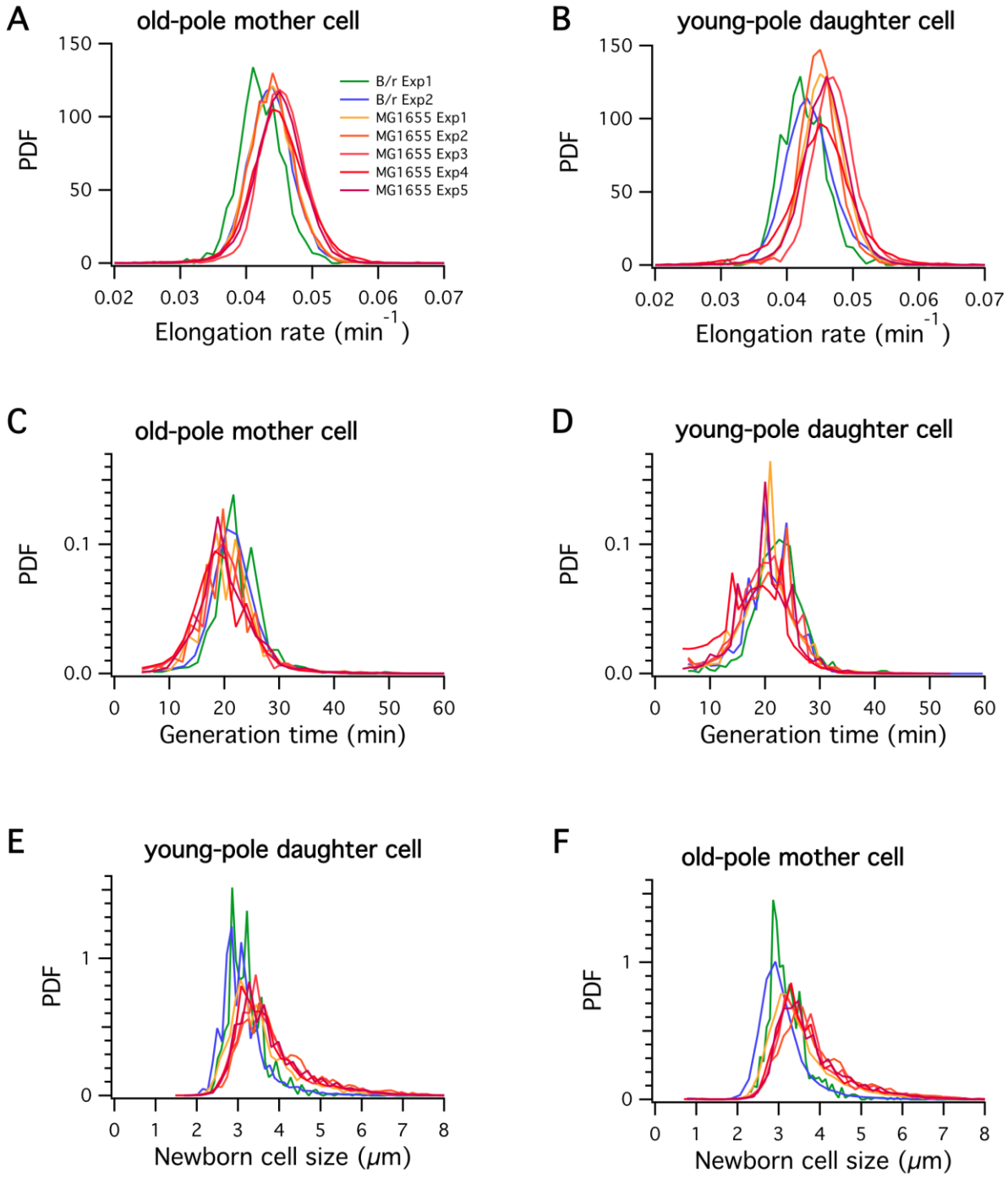

A. Elongation rate (old-pole mother cell)

Exp \ Stat	Avg (1/mins)	Var (1/mins)	# cells
B/r Exp1	0.043	0.003	1008
B/r Exp2	0.044	0.006	16585
MG1655 Exp1	0.044	0.004	11412
MG1655 Exp2	0.044	0.005	3650
MG1655 Exp3	0.046	0.005	3005
MG1655 Exp4	0.045	0.006	20961
MG1655 Exp5	0.045	0.005	22959

B. Elongation rate (young-pole daughter cell)

Exp \ Stat	Avg (1/mins)	Var (1/mins)	# cells
B/r Exp1	0.043	0.004	1008
B/r Exp2	0.044	0.004	16585
MG1655 Exp1	0.046	0.004	11412
MG1655 Exp2	0.045	0.003	3650
MG1655 Exp3	0.047	0.004	3005
MG1655 Exp4	0.046	0.005	20961
MG1655 Exp5	0.046	0.007	22959

C. Generation time (old-pole mother cell)

Exp \ Stat	Avg (mins)	Var (mins)	# cells
B/r Exp1	23.4	4.8	1008
B/r Exp2	22.8	4.8	16585
MG1655 Exp1	21.4	5	11412
MG1655 Exp2	21.4	5.7	3650
MG1655 Exp3	20.8	5.9	3005
MG1655 Exp4	20.3	5.3	20961
MG1655 Exp5	21.4	5.4	22959

D. Generation time (young-pole daughter cell)

Exp \ Stat	Avg (mins)	Var (mins)	# cells
B/r Exp1	22.8	4.7	1008
B/r Exp2	21.4	4.7	16585
MG1655 Exp1	21	4.9	11412
MG1655 Exp2	20.8	5.5	3650
MG1655 Exp3	20.4	5.1	3005
MG1655 Exp4	18.1	5.7	20961
MG1655 Exp5	20.4	5	22959

E. Newborn cell size (old-pole mother cell)

Exp \ Stat	Avg (μm)	Var (μm)	# cells
B/r Exp1	3.3	0.6	1008
B/r Exp2	3.3	1.1	16585
MG1655 Exp1	3.6	1	11412
MG1655 Exp2	4.1	1.3	3650
MG1655 Exp3	3.9	1.2	3005
MG1655 Exp4	3.8	1	20961
MG1655 Exp5	3.9	1.1	22959

F. Newborn cell size (young-pole daughter cell)

Exp \ Stat	Avg (μm)	Var (μm)	# cells
B/r Exp1	3.3	0.6	1008
B/r Exp2	3.3	0.7	16585
MG1655 Exp1	3.4	0.8	11412
MG1655 Exp2	3.8	1	3650
MG1655 Exp3	3.7	0.9	3005
MG1655 Exp4	3.6	0.8	20961
MG1655 Exp5	3.7	0.9	22959

Table of statistics of growth. (avg = average, var = variance) (**a, b**) elongation rate (**c, d**) generation time (**e, f**) newborn cell size

Figure S2, related to Figure 2. Statistics of the pairwise difference between the mother and the daughter cells measured by (daughter - mother)/mother. B/r and MG1655. (**A, B**) elongation rate (**C, D**) generation time (**E, F**) newborn cell size. In the tables, avg = average and var = variance.

A

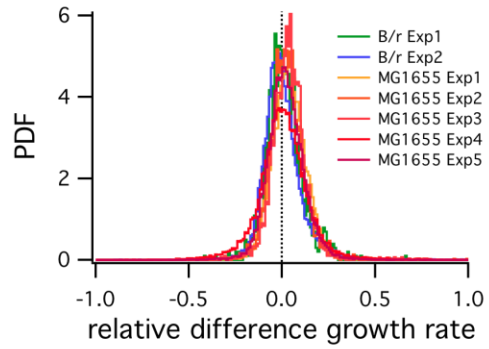

Exp \ Stat	Avg	Var	# cells
B/r Exp1	-0.003	0.109	2016
B/r Exp2	-0.019	0.108	33170
MG1655 Exp1	0.029	0.12	22824
MG1655 Exp2	0.016	0.108	7300
MG1655 Exp3	0.028	0.104	6010
MG1655 Exp4	0.0003	0.147	41922
MG1655 Exp5	0.01	0.12	45918

B

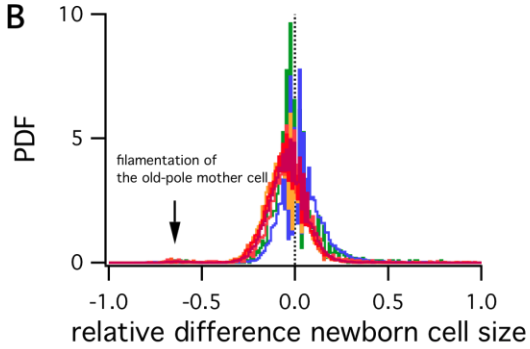

Exp \ Stat	Avg	Var	# cells
B/r Exp1	-0.002	0.137	2016
B/r Exp2	0.049	0.351	33170
MG1655 Exp1	-0.029	0.29	22824
MG1655 Exp2	-0.029	0.29	7300
MG1655 Exp3	-0.013	0.242	6010
MG1655 Exp4	-0.037	0.337	41922
MG1655 Exp5	-0.02	0.349	45918

C

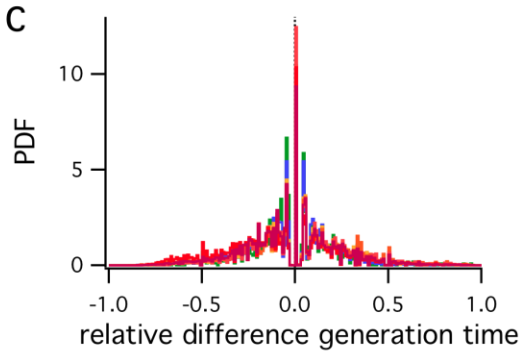

Exp \ Stat	Avg	Var	# cells
B/r Exp1	-0.0002	0.238	2016
B/r Exp2	-0.034	0.255	33170
MG1655 Exp1	0.0145	0.311	22824
MG1655 Exp2	0.0145	0.311	7300
MG1655 Exp3	0.032	0.339	6010
MG1655 Exp4	-0.068	0.33	41922
MG1655 Exp5	-0.014	0.275	45918

Figure S3, related to Figure 3. Filamentation rate of MG1655 (A), MG1655 *lexA*3 mutant (no SOS) (B) and B/r (C). We included Fig. 3C here for convenience of the reader. Note that the filamentation rate of the lexA3 mutant is significantly suppressed, i.e., the much higher filamentation rate of MG1655 is likely SOS-dependent. As for B/r, we note that this strain lacks one of the key SOS genes, sulA, which inhibits cell division during the SOS response. This may explain the low filamentation rate of this strain.

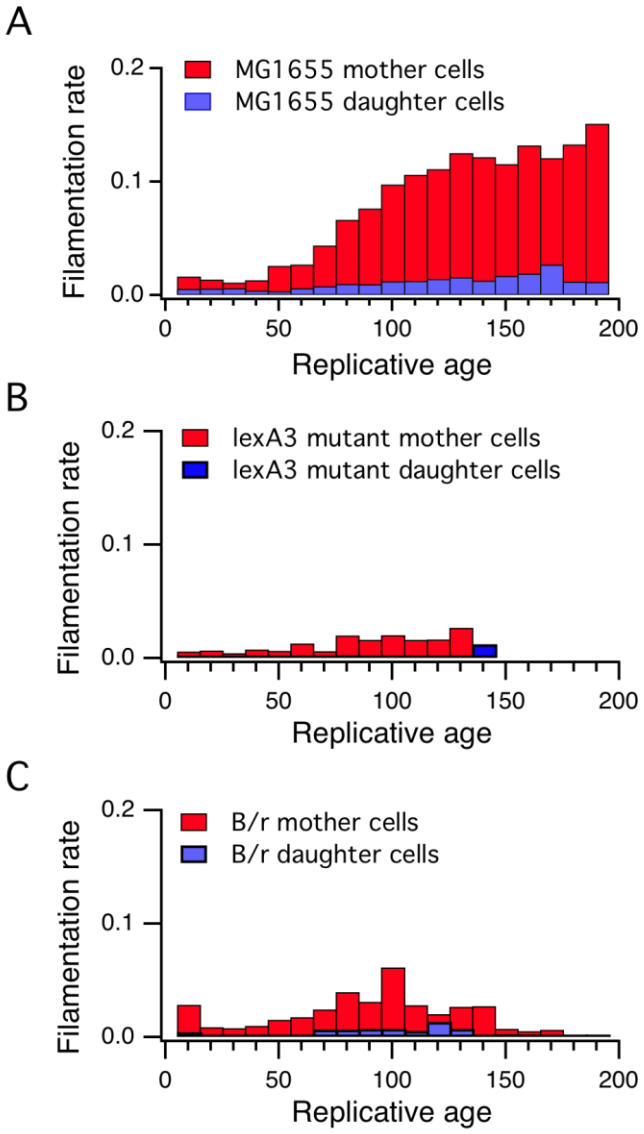

Figure S4. Control experiments that show separation of timescales between diffusion of small molecules in the growth channel (fast) and nutrient uptake of the cell (slow). **(A)** Timeseries of *E. coli* cells in the growth channels during nutrient shift-down from LB to M9-minimal medium containing a fluorescent glucose analog [2-NBDG; Yoshioka *et al*, *Biosci. Biotechnol. Biochem.* **60**(11), 1899-1901 (1996); Natarajan & Srienc, *J. Microbiol. Meth*. **42**, 87-96 (2000)]. After nutrient-shift, weak fluorescence starts to appear in the first 20 seconds and becomes visible in 40 seconds. Fluorescent intensities of the cells at different positions along the growth channel increase simultaneously, i.e., the diffusion of the small molecules in the growth channel is much faster than the uptake rate of cells, (B) Uptake rate of fluorescent glucose analog (2-NBDG) and timescale of diffusion of nanoparticles in the growth channel. The fluorescence level of the cells increases steadily and reaches a plateau. The median timescale is ~150 seconds. (C) Timescale of diffusion of nanoparticles in the growth channels. We filled both the main trench and the growth channels of our device with fluorescent nanoparticles of diameter 38nm (G40, company name here). Then, we instantaneously removed the particles in the main trench with a fast flow of water. Accordingly, the particles in the growth channels escaped to the main trench by diffusion. The median timescale of diffusion is about 10 seconds measured by the decrease of fluorescent intensity integrated in the growth channel area. Since the diffusion constant D is inversely proportional to the size of the particle (the Stoke's law), we estimate the timescale of diffusion for particles of the size of typical proteins or metabolites (e.g., 4nm for GFP) to be of order ~1 second. This two orders of magnitude separation of timescales between diffusion and nutrient uptake ensures that the cells in the growth channels are under constant level of nutrient; and also that there is no accumulation of the small molecules in the growth channels.

Additional Note:

To ensure the cells in this experiment were in steady state in the fluorescent glucose uptake experiment, cells were first grown in the growth channels in LB at 37°C for more than 10 generations. Then, M9 minimal medium containing fluorescent glucose (2-NBDG) was infused into the channels to replace LB immediately. A highly sensitive EM-CCD camera was used for imaging (Hamamatsu EM-CCD 9100-13).

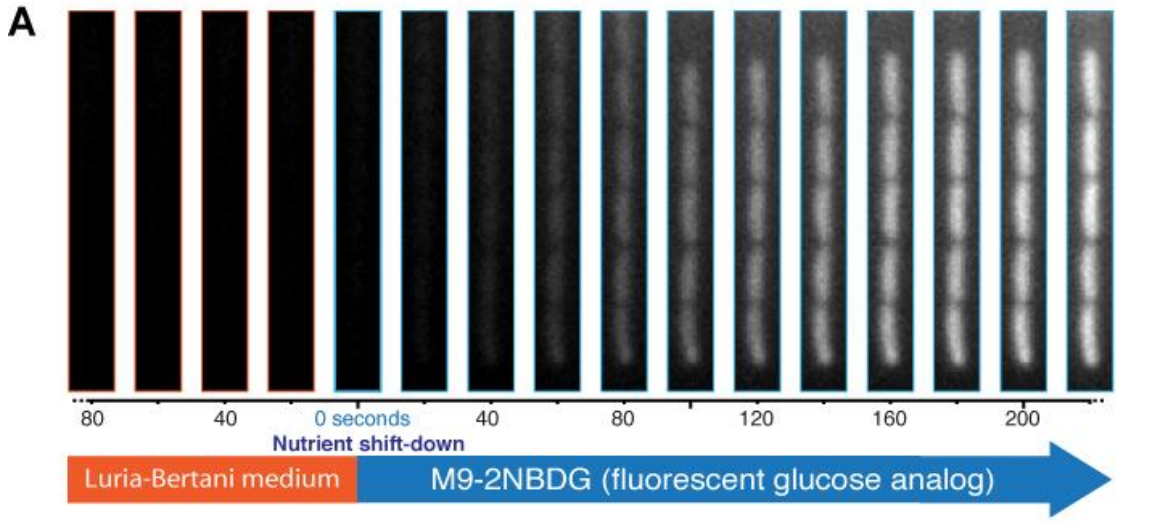
A
80
40
0 seconds
40
80
120
160
200
Nutrient shift-down
Luria-Bertani medium
M9-2NBDG (fluorescent glucose analog)

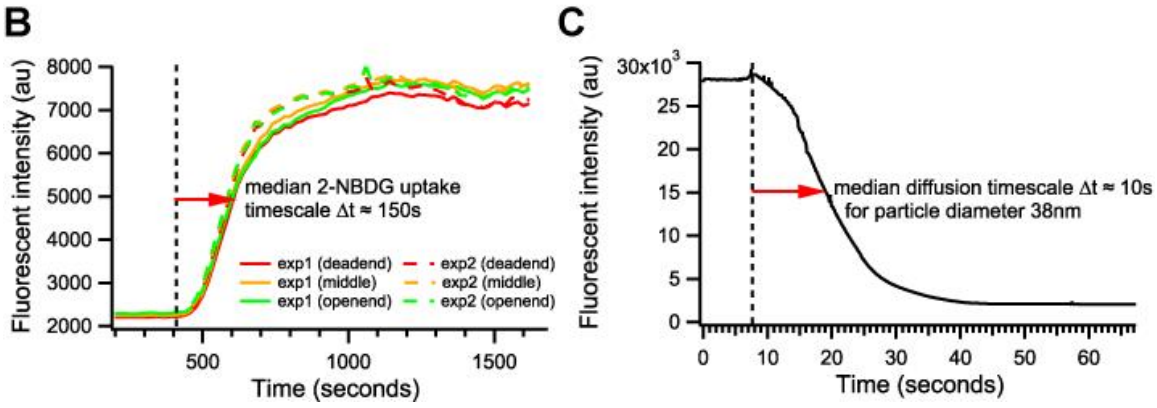
B
Fluorescent intensity (au)
8000
7000
6000
5000
4000
3000
2000
median 2-NBDG uptake
timescale Δt ≈ 150s
exp1 (deadend)
exp1 (middle)
exp1 (openend)
exp2 (deadend)
exp2 (middle)
exp2 (openend)
500
1000
1500
Time (seconds)
C
Fluorescent intensity (au)
30x10^3
25
20
15
10
5
0
median diffusion timescale Δt ≈ 10s
for particle diameter 38nm
0
10
20
30
40
50
60
Time (seconds)

Supplemental Experimental Procedures

Design of the mother machine. We used a standard soft lithography techniques pioneered by George Whitesides and others. We used a SU8 photoresist to make the master mould in two steps (the first layer for the growth channels and the second layer for the main trench), and Polydimethylsiloxane (PDMS) to make the mother machine. The dimensions of the growth channels are approximately 25µm (L) x 1.5µm (W) x 1.4µm (D), which are connected to a main trench of varying length and width. To enable long-term observation of the growth of *E. coli*, we chemically treated the PDMS device using a protocol similar to Supplemental Ref. [1]. In addition, the PDMS surface was passivated with 10mg/ml BSA and 0.1% of BSA was used in the LB background to prevent cell adhesion to the PDMS surface.

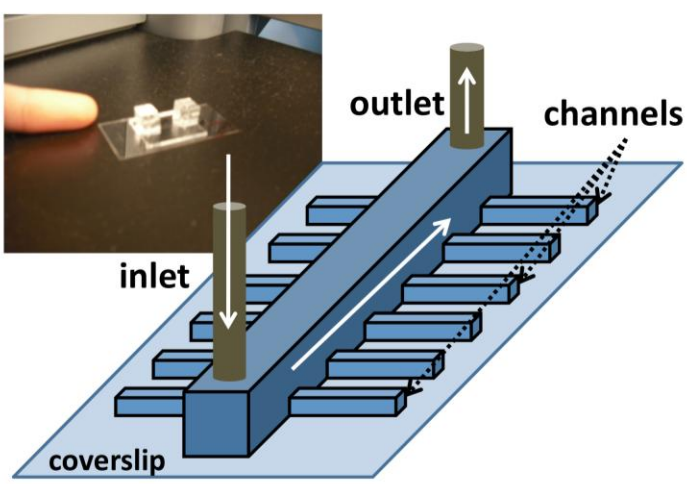

DIMENSIONS

channel width, height
~ 1 µm
channel length
~ 25 µm
trench depth x width
(not to scale)
~ 25µm x 100 µm
trench length
~ 30 mm

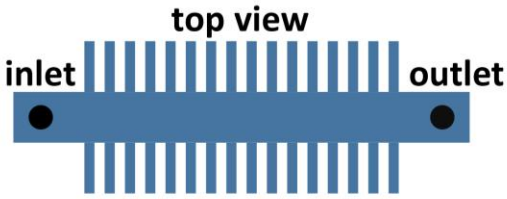

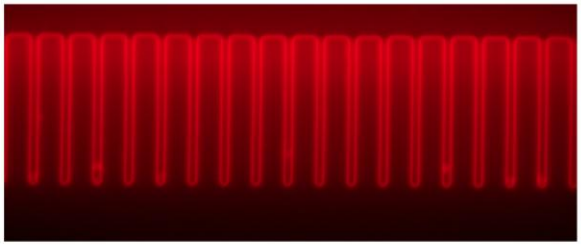

Construction of the lineage tree by growing cells in the mother machine. (A) The lifecycle of *E. coli* in the growth channel. Since the fraction of the cell in the population decreases exponentially with the age of the pole as $1/2^n$, where n is the age of the old pole, the growth channels are most likely to be filled with very young cells upon initial loading of the cells. (B) Lineage tree of the growing *E. coli* in mother machine. Red and blue branches indicate old-pole mother cell at dead end of channel and young-pole daughter cell respectively.

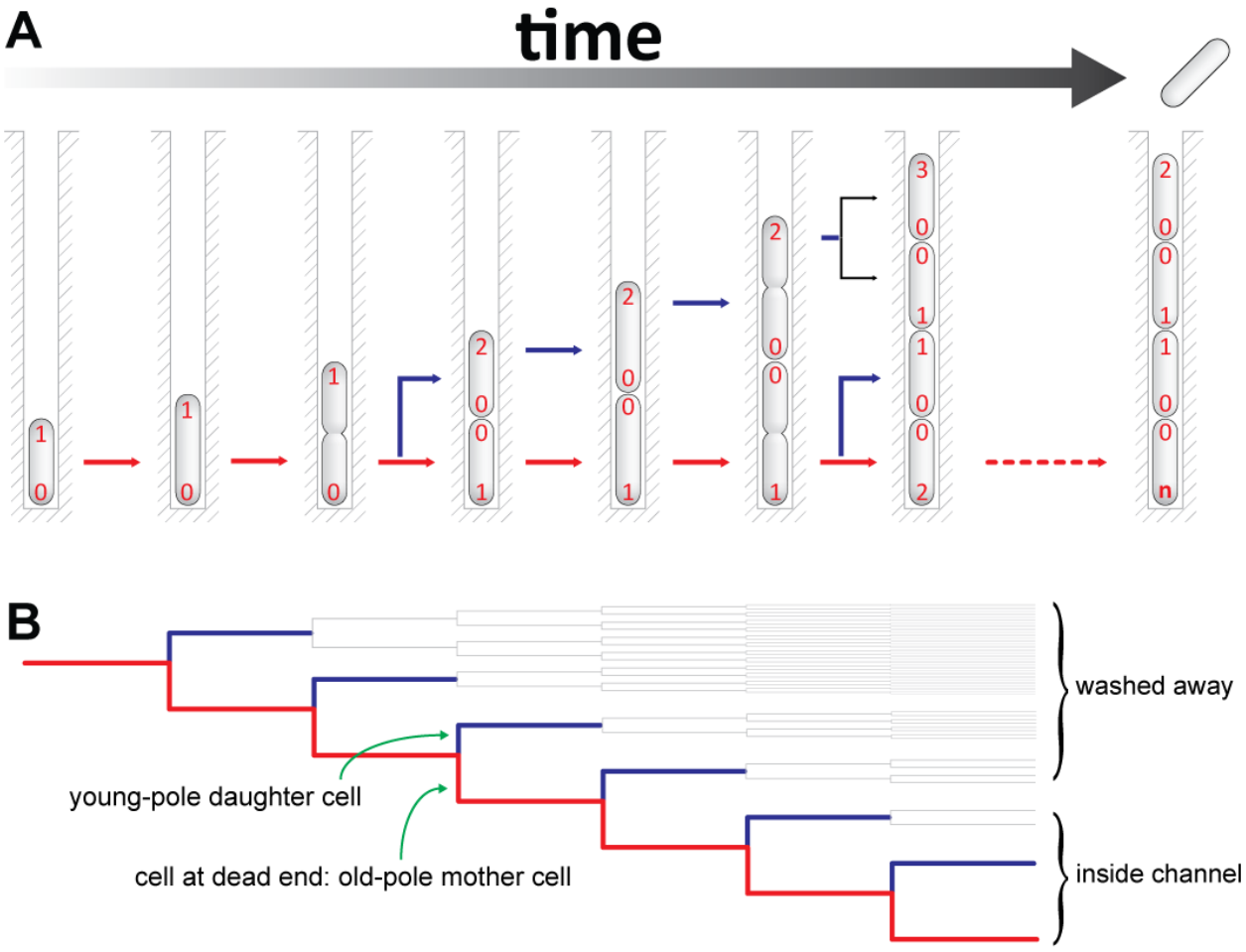

Author Contributions

SJ conceived and supervised the project. WLD, SJ and LR developed the experimental protocol. WLD and SJ designed the microfluidic "mother machine" and jointly constructed the device with PW. LR and AW constructed the strains. SJ and JP initiated image analysis method, and PW wrote CellTracker software used in the study. WLD,

SJ, JP, LR and PW performed experiments and SJ, JP and PW analyzed the data. SJ wrote the paper with AW. All authors discussed the results and implications and commented on the manuscript.

Supplemental References

1. Lee, J. Ng, Park, C., Whitesides, G. M. (2003). Solvent compatibility of poly(dimethylsiloxane)-based microfluidic devices. *Anal. Chem. 75*, 6544-6554.